

Water-wave propagation through an infinite array of cylindrical structures

By P. McIVER

Department of Mathematical Sciences, Loughborough University,
Loughborough, Leicestershire, LE11 3TU, UK

(Received 13 September 1999 and in revised form 9 June 2000)

An investigation is made into water-wave propagation through an array of vertical cylinders extending to infinity and periodic in both horizontal directions. Methods are presented for the calculation of the frequency ranges for which wave propagation without change of amplitude is possible ('passing bands'), and for which propagation without change of amplitude is not possible ('stopping bands'). Some of the techniques may be used to determine the change of wave amplitude for frequencies within the stopping bands. Approximate and numerical techniques are used to show how this infinite-array problem is related to trapped modes, Rayleigh–Bloch waves, and the problem of wave diffraction by a grating made up of a finite number of cylinder rows.

1. Introduction

The problem of a particle moving in a periodic potential has been studied extensively in solid-state physics and there is an established formalism for its investigation (Ashcroft & Mermin 1976). A mathematically related problem is the propagation of water waves above a patch of sea bed with undulations that are periodic in one horizontal direction (see O'Hare & Davies 1993, and references therein). Given a particular sea bed, it is observed that there are ranges of frequency where there is strong reflection, and complementary ranges for which there is weak reflection, of a monochromatic incident wave. Recently, Chou (1998) has considered water-wave interaction with an infinite array of periodically arranged surface scatterers using the formalism of solid-state physics. He investigated geometries that are periodic in both one and two horizontal directions and found that for certain ranges of frequency wave propagation through the array without change in amplitude is possible, although in general there will be a change in phase from one scatterer to another. In complementary ranges of frequency, wave propagation without change of amplitude is not possible. In the terminology of solid-state physics, these ranges of frequency are known as passing bands and stopping bands, respectively. Similar phenomena have been observed in other systems such as the propagation through periodic media of electromagnetic waves (e.g. McCall *et al.* 1991), and elastic and acoustic waves (e.g. Sigalas & Economou 1992). Mention might also be made of the extensive literature on lattice sums (e.g. Chin, Nicorovici & McPhedran 1994) which may be used for computational purposes in such problems.

In this paper, the propagation of water waves through an array of identical vertical cylinders that is periodic on both horizontal directions is examined in detail. This

work is motivated in part by a proposal for a airport in Japan that involves a floating platform supported by thousands of cylindrical legs. Over recent years, this has provoked interest in how water waves interact with very large arrays of vertical cylinders (Kagemoto & Yue 1986; Kagemoto 1998; Kashiwagi 2000). The main purpose of the work described here is to investigate how knowledge of the relatively straightforward problem of wave propagation through infinite arrays of cylinders can be used to make deductions about propagation through finite arrays. Although set into the context of water waves, the present work also has an acoustic interpretation and related work on sound propagation through tube bundles is reported by Heckl & Mulholland (1995).

In this paper the problem is treated on the basis of inviscid, linear theory. (Kashiwagi 2000 reports comparisons of numerical calculations based on this theory with experimental data for scattering by an array of 64 cylinders and obtains good qualitative agreement.) The problem is formulated in §2 in terms of a velocity potential for the flow. Because of the periodic arrangement of cylinders, it is possible to confine attention to a cell in a horizontal plane that contains only a single cylinder. For a rectangular array this primitive cell is also rectangular and so-called Bloch conditions are used to relate the potential and its normal derivative on opposite sides of the rectangle. Throughout this paper the problem of wave propagation through an infinite array will be referred to as 'the Bloch problem'. An approximate solution of the Bloch problem for unidirectional wave propagation is presented in §3. This is used to show how passing and stopping bands arise in the water-wave problem. Within a passing band waves are able to propagate through the array without change of amplitude. Within stopping bands there is change in wave amplitude with distance.

For a passing band the boundary-value problem is self-adjoint and the frequencies can be calculated quite straightforwardly by means of a variational principle. This method is used in §4 to investigate how the band structure develops as the cylinder radius is increased from zero. In addition, calculations are presented to show how the solutions obtained approach previously known trapped mode and Rayleigh–Bloch wave solutions as one of the cell dimensions is allowed to increase without bound. In this context, the term Rayleigh–Bloch wave is used to describe a non-periodic wave that propagates along an infinitely long line of equally spaced cylinders and decays to zero in the perpendicular horizontal direction. The term trapped mode is here reserved for certain limiting cases when the solution and the geometry have the same periodicity.

The variational method of §4 gives no information about the rate of change of amplitude with distance for frequencies within stopping bands. Two numerical methods which calculate this rate of change are given in §5. In the first method, a series that satisfies the cylinder boundary condition identically is applied pointwise to satisfy the conditions on the cell walls. This method is straightforward to use but is not very robust for higher frequencies. The second technique is a more robust, but also more computationally expensive, boundary-integral method based on an application of Green's theorem.

The final sections of the paper deal with wave diffraction by a finite number of parallel rows of cylinders, where each row is of infinite length. In §6, a wide-spacing formulation is used to demonstrate explicitly how, for the case of wave propagation normal to the rows, the transmission beyond a finite number of rows is related to the Bloch problem. In §7, various numerical calculations using the methods of §§4–5 are used to investigate the finite-array problem when waves are able to propagate in more than one direction.

2. General formulation

A periodic array of identical, rigid, circular cylinders, which extend to infinity in all horizontal directions, stands in water of constant depth h . Cartesian coordinates are chosen so that the x - and y -axes lie in a horizontal plane and the z -axis is directed vertically upwards. The origin of coordinates is on the axis of one of the cylinders and located in the plane of the mean free surface. Water waves of radian frequency ω propagate through the array. The water is assumed to be inviscid and incompressible and the flow to be irrotational. The cylinders extend throughout the depth and so, under the usual assumptions of the linearized theory of water waves, solutions for the velocity potential may be sought in the form

$$\Phi(x, y, z, t) = \text{Re} \{ \phi(x, y) \cosh \kappa(z + h) e^{-i\omega t} \}, \quad (1)$$

where

$$(\nabla^2 + \kappa^2)\phi = 0 \quad (2)$$

throughout the now two-dimensional fluid region, and κ is the real positive root of the dispersion relation

$$\omega^2 = g\kappa \tanh \kappa h. \quad (3)$$

Ultimately in this paper, interest will be in scattering problems that are forced by an incident wave with wavenumber κ that has the same depth dependence as the form in equation (1). Other possible forms of the depth dependence in (1) are not relevant to a scattering problem because of the orthogonality properties of the vertical eigenfunctions in the linearized water-wave problem.

The geometrical description of the array (or lattice) of cylinders adopted here is that used in the theory of crystal structures in solid-state physics (see Ashcroft & Mermin 1976, Chapters 4 and 5). Let \mathbf{a}_1 and \mathbf{a}_2 be two vectors that span the lattice: that is every translation between the axes of cylinders in the horizontal plane has the form of a so-called lattice vector

$$\mathbf{R} = m_1 \mathbf{a}_1 + m_2 \mathbf{a}_2, \quad (4)$$

where m_1 and m_2 are integers. It is also convenient to introduce so-called reciprocal lattice vectors \mathbf{K} satisfying

$$\mathbf{K} \cdot \mathbf{R} = 2\pi p \quad (5)$$

where p is an integer. If the reciprocal lattice vectors are expressed in the form

$$\mathbf{K} = n_1 \mathbf{b}_1 + n_2 \mathbf{b}_2 \quad (6)$$

for integers n_1, n_2 then (5) is satisfied provided

$$\mathbf{a}_i \cdot \mathbf{b}_j = 2\pi \delta_{ij}, \quad (7)$$

where δ_{ij} is the Kronecker delta.

In other contexts (Ashcroft & Mermin 1976, Chapter 8; Chou 1998), Bloch's theorem is used to justify looking for solutions in the form

$$\phi(\mathbf{r}) = e^{i\mathbf{q} \cdot \mathbf{r}} \psi(\mathbf{r}), \quad (8)$$

where \mathbf{r} is the position vector of an arbitrary point in the array, \mathbf{q} is a real-valued vector, and the function ψ has the same periodicity as the lattice, that is

$$\psi(\mathbf{r} + \mathbf{R}) = \psi(\mathbf{r}) \quad (9)$$

for all lattice vectors \mathbf{R} . Here solutions are also sought in this form, but in the

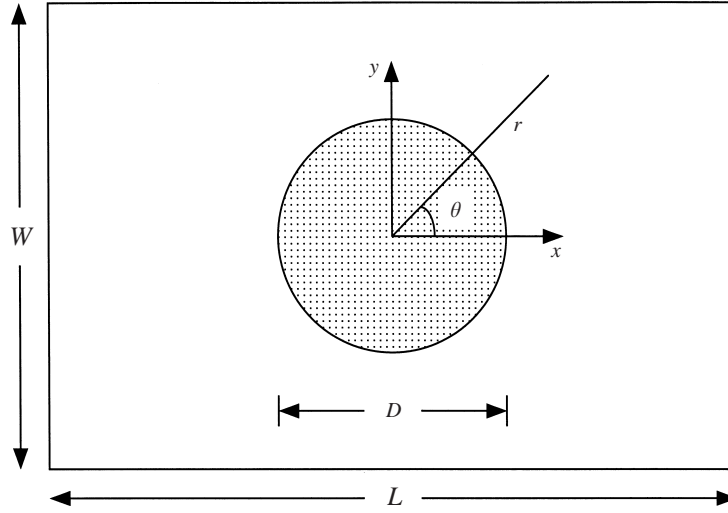


FIGURE 1. Definition sketch for one cell of a rectangular array.

water-wave problem \mathbf{q} may be complex. The above is exactly equivalent to seeking solutions that satisfy

$$\phi(\mathbf{r} + \mathbf{R}) = e^{i\mathbf{q}\cdot\mathbf{R}}\phi(\mathbf{r}), \quad (10)$$

where \mathbf{R} is again any lattice vector. The real part of \mathbf{q} measures the change in the phase of the motion as the lattice is traversed. If \mathbf{q} has a non-zero imaginary part then there is also a change in amplitude as a wave propagates through the array.

Two basic approaches to the problem are used here. One approach is to specify the wave vector $\mathbf{q} = q_1\mathbf{i} + q_2\mathbf{j}$ and then to solve for the wavenumber κ (here \mathbf{i} and \mathbf{j} are unit vectors in the x - and y -directions, respectively). Alternatively, κ and one component of \mathbf{q} is specified and the problem is then to determine the second component of \mathbf{q} .

For a rectangular array of cylinders of diameter D with

$$\mathbf{a}_1 = L\mathbf{i} \quad \text{and} \quad \mathbf{a}_2 = W\mathbf{j} \quad (11)$$

it is sufficient to consider a single rectangular cell of length L and width W as illustrated in figure 1. The corresponding primitive reciprocal lattice vectors are

$$\mathbf{b}_1 = \frac{2\pi\mathbf{i}}{L} \quad \text{and} \quad \mathbf{b}_2 = \frac{2\pi\mathbf{j}}{W}. \quad (12)$$

For this geometry, equation (10) is equivalent to the four independent conditions

$$\left. \begin{aligned} \phi(L/2, y) &= e^{iq_1L} \phi(-L/2, y), \\ \frac{\partial\phi}{\partial x}(L/2, y) &= e^{iq_1L} \frac{\partial\phi}{\partial x}(-L/2, y), \end{aligned} \right\} |y| \leq W/2, \quad (13)$$

$$\left. \begin{aligned} \phi(x, W/2) &= e^{iq_2W} \phi(x, -W/2), \\ \frac{\partial\phi}{\partial y}(x, W/2) &= e^{iq_2W} \frac{\partial\phi}{\partial y}(x, -W/2), \end{aligned} \right\} |x| \leq L/2. \quad (14)$$

The mathematical problem has been reduced to the solution of the field equation (2)

within the two-dimensional fluid region of the cell $\{|x| \leq L/2, |y| \leq W/2\}$ subject to the boundary conditions (13)–(14) and the condition of no flow through the cylinder wall, namely

$$\frac{\partial \phi}{\partial r} = 0 \quad \text{on} \quad r = D/2, \quad (15)$$

where (r, θ) are standard plane polar coordinates with origin at the centre of the primitive cell illustrated in figure 1.

Equation (10) is unchanged if \mathbf{q} is augmented by any reciprocal lattice vector \mathbf{K} . Thus, given a solution $\phi(\mathbf{r}; \mathbf{q})$ then $\phi(\mathbf{r}; \mathbf{q} + \mathbf{K})$ is also a solution. Consequently, it is sufficient to restrict attention to the so-called ‘first Brillouin zone’ $\{\text{Re } q_1 L \in [-\pi, \pi], \text{Re } q_2 W \in [-\pi, \pi]\}$, as long as it is born in mind that for any pair (κ, \mathbf{q}) , for which the problem has a non-trivial solution, such solutions also exist for pairs $(\kappa, \mathbf{q} + \mathbf{K})$. This method of displaying results is known as a ‘reduced zone scheme’ (Ashcroft & Mermin 1976, p. 160).

3. A wide-spacing approximation

To illustrate clearly some important features of the problem defined by equations (2) and (13)–(15) an approximate solution is now presented for the case $q_2 = 0$. The main assumption is that the cell length in the x -direction is much greater than the wavelength so that $\kappa L \gg 1$. In other words, for the corresponding infinite array the spacing between those rows oriented parallel to the y -axis is large compared to the wavelength. Further, only solutions symmetric about $y = 0$ are considered and the boundary conditions (14) are replaced by the special case

$$\frac{\partial \phi}{\partial y} = 0 \quad \text{on} \quad y = \pm W/2, \quad (16)$$

which is equivalent to having solid channel walls at $y = \pm W/2$. The conditions (13) are retained in their general form. It will also be assumed that the wavenumber satisfies $\kappa W < 2\pi$ so that only waves with no y dependence may propagate in a channel of width W . The main aim is to calculate the so-called Bloch transmission coefficient

$$T_B = e^{iq_1 L} \quad (17)$$

which measures the changes in phase and amplitude of a wave as it propagates through one cell of the array in the direction of x increasing (see equations (13)).

If the length L of the cell is sufficiently large then only plane waves propagating along the channel can exist in the vicinity of $x = \pm L/2$; evanescent modes of the form

$$\exp(\mp[(2m\pi/W)^2 - \kappa^2]^{1/2} x) \cos(2m\pi y/W), \quad m = 1, 2, 3, \dots,$$

will be negligible in these regions. Thus, in the neighbourhood of $x = -L/2$,

$$\phi = A_1 e^{i\kappa x} + B_1 e^{-i\kappa x}, \quad (18)$$

and in the neighbourhood of $x = L/2$,

$$\phi = A_2 e^{i\kappa x} + B_2 e^{-i\kappa x}, \quad (19)$$

for some complex constants A_1, A_2, B_1 and B_2 . The wave with amplitude A_2 propagates away from the cylinder and is due to the transmission of A_1 past the cylinder and the reflection of B_2 from the cylinder. Similarly, the wave with amplitude B_1 arises from

the transmission of B_2 and the reflection of A_1 . Thus

$$A_2 = TA_1 + RB_2 \quad \text{and} \quad B_1 = TB_2 + RA_1, \quad (20)$$

where R and T are the reflection and transmission coefficients for a single cylinder in the channel (cf. Heckl 1992, equations 37). The boundary conditions (15) and (16) are used in the calculation of R and T , which are assumed to be known for all κ . The Bloch conditions (13) give

$$A_2 = A_1 e^{i(q_1 - \kappa)L} \quad \text{and} \quad B_2 = B_1 e^{i(q_1 + \kappa)L} \quad (21)$$

which when combined with equations (20) yield

$$\mathbf{s} \begin{pmatrix} A_1 \\ B_1 \end{pmatrix} = T_B \begin{pmatrix} A_1 \\ B_1 \end{pmatrix} \quad (22)$$

where $T_B = e^{iq_1 L}$ and

$$\mathbf{s} = \begin{pmatrix} (T - R^2/T)e^{i\kappa L} & Re^{i\kappa L}/T \\ -Re^{-i\kappa L}/T & e^{-i\kappa L}/T \end{pmatrix} \quad (23)$$

is the so-called scattering matrix which appears in the scattering problem described in §6. The allowable values of T_B are just the eigenvalues of \mathbf{s} which are given by the roots of

$$T_B^2 T e^{-i\kappa L} - T_B (T^2 - R^2 + e^{-2i\kappa L}) + T e^{-i\kappa L} = 0. \quad (24)$$

If the complex number T is expressed in the form

$$T = |T|e^{i\delta} \quad (25)$$

then it may be shown that

$$R = |R|e^{i(\delta \pm \pi/2)} \quad (26)$$

(Mei 1983, §7.6.2, describes the derivation for the purely two-dimensional case, the channel case is a trivial extension). Use of these relations and the energy relation

$$|R|^2 + |T|^2 = 1, \quad (27)$$

all valid below the cut-off wavenumber $\kappa W = 2\pi$, allows the above quadratic to be rewritten as

$$T_B^2 - \frac{2 \cos(\delta + \kappa L)}{|T|} T_B + 1 = 0. \quad (28)$$

By a standard result for quadratic equations, the product of the roots is unity so that if $e^{iq_1 L}$ is a root then so is $e^{-iq_1 L}$. The sum of the roots then yields

$$\cos q_1 L = \frac{\cos(\delta + \kappa L)}{|T|} \equiv f(\kappa L), \quad (29)$$

say (cf. Ashcroft & Mermin 1976, p. 148), which is an equation for $q_1 L$ entirely in terms of real quantities. It is perhaps helpful to think of κ as the 'local' wavenumber of propagating modes while q_1 governs the phase and amplitude variation of these modes as they propagate through the array. Provided $|f(\kappa L)| \leq 1$, equation (29) has only real solutions for $q_1 L$ and waves will propagate through the array with their amplitude unchanged. The ranges of frequency for which this occurs are known in solid-state physics as 'passing bands'. However, whenever $|f(\kappa L)| > 1$ solutions are of the form $q_1 L = n\pi \pm iQ$ for real $Q > 0$ and some integer n (in the reduced-zone scheme

$n = 0$ or $n = \pm 1$). The ranges of frequency for which propagation without change of amplitude is impossible are known in solid-state physics as ‘stopping bands’.

In contrast to the application of this theory to crystal lattices, complex \mathbf{q} in the water-wave problem has a physical interpretation. Further discussion of this is given later in § 5.1 where a method for the computation of complex \mathbf{q} is presented. The next section is devoted to a method of computation valid for real \mathbf{q} only.

4. Numerical calculations for the passing bands

Attention is now turned to numerical methods for the calculation of solutions to the problem defined by equations (2) and (13)–(15). In this section real values of the Bloch wave vector $\mathbf{q} = \{q_1, q_2\}$ are considered; such values correspond to the passing bands introduced in § 3 in which waves are able to propagate through an infinite array without change of amplitude.

A computational method for the passing bands based on a variational formulation is presented in § 4.1. Results are given in § 4.2 that show how the stopping bands develop as the cylinder size is increased. The connections between the Bloch problem and previously known solutions for trapped and Rayleigh–Bloch waves are discussed in §§ 4.3 and 4.4, respectively.

4.1. Variational formulation of the eigenvalue problem

For a specified real Bloch wave vector $\mathbf{q} = \{q_1, q_2\}$ the problem is self-adjoint and the corresponding infinite sequence of eigenvalues $\lambda = \kappa^2$ of the negative Laplacian may be determined by a standard application of the Rayleigh–Ritz method (see, for example, Duff & Naylor 1966, Chapter 6). The Rayleigh quotient for a given trial function u is

$$\mathcal{R}(u) = \frac{\int_A |\nabla u|^2 dA}{\int_A |u|^2 dA}, \quad (30)$$

where A is the two-dimensional fluid domain within the horizontal cross-section illustrated in figure 1. The Neumann condition (15) is a ‘natural’ boundary condition and need not be incorporated into the trial function u . However, it is essential that u satisfies the Bloch condition (10). This is achieved by writing

$$u = \sum_{m,n=-P}^P A_{mn} e^{i(\mathbf{q} + \mathbf{K}_{mn}) \cdot \mathbf{r}} \quad (31)$$

where

$$\mathbf{K}_{mn} = 2\pi \left(\frac{m}{L} \mathbf{i} + \frac{n}{W} \mathbf{j} \right) \quad (32)$$

is a reciprocal lattice vector, as defined in equation (5), and $\mathbf{r} = x\mathbf{i} + y\mathbf{j}$ is the position vector of an arbitrary point in A . Approximations to the eigenvalues correspond to the local minima of $\mathcal{R}(u)$ with respect to variations in the coefficients A_{mn} . This leads to the generalized eigenvalue problem

$$\sum_{m,n=-P}^P (\mathcal{E}_{klmn} - \lambda \mathcal{H}_{klmn}) = 0, \quad k, l = -P, \dots, P, \quad (33)$$

for λ where

$$\mathcal{H}_{klmn} = \int_A e^{i(\mathbf{K}_{kl} - \mathbf{K}_{mn}) \cdot \mathbf{r}} dA = \begin{cases} -\frac{\pi D}{\alpha_{klmn}} J_1\left(\frac{1}{2} D \alpha_{klmn}\right), & k \neq m \text{ and } l \neq n, \\ WL - \frac{1}{4} \pi D^2, & k = m \text{ and } l = n, \end{cases} \quad (34)$$

$$\begin{aligned} \mathcal{E}_{klmn} &= [(q_1 + 2\pi k/L)(q_1 + 2\pi m/L) \\ &\quad + (q_2 + 2\pi l/W)(q_2 + 2\pi n/W)] \int_A e^{i(\mathbf{K}_{kl} - \mathbf{K}_{mn}) \cdot \mathbf{r}} dA \\ &= [(q_1 + 2\pi k/L)(q_1 + 2\pi m/L) + (q_2 + 2\pi l/W)(q_2 + 2\pi n/W)] \mathcal{H}_{klmn}, \end{aligned} \quad (35)$$

$$\alpha_{klmn} = 2\pi \left(\frac{(k-m)^2}{L^2} + \frac{(l-n)^2}{W^2} \right)^{1/2}, \quad (36)$$

and J_1 denotes the Bessel function of the first kind and order one.

The eigenvalue problem is solved using standard numerical techniques. The value of P required to achieve a particular accuracy depends on the parameters W/L and D/L . Most of the calculations in this paper are for $W/L = 1$ and $D/L = 0.5$; in this case $P = 12$ is sufficient to obtain at least seven-figure accuracy for the twelve smallest eigenvalues. Smaller values of D/L or values of W/L significantly different from unity require larger values of P .

Although the above formulation uses q_1 and q_2 as input and then solves for κ , it is relatively straightforward to adapt the technique to use q_2 and κ as input and then solve for q_1 . Let $\{\kappa_i(q_1, q_2), i = 1, 2, \dots\}$ denote the set of the square roots of the eigenvalues λ corresponding to specified values of q_1 and q_2 . Fix q_2 and for the chosen κ define

$$f(q_1; \kappa, q_2) = \min_i |\kappa - \kappa_i(q_1, q_2)|. \quad (37)$$

Now determine the local minima of $f(q_1; \kappa, q_2)$ as a function of $q_1 \in [0, \pi/L]$. If a minimum of $f(q_1; \kappa, q_2)$ is zero (within some tolerance), then the corresponding value of q_1 is a solution (there may be more than one such q_1). If the global minimum of $f(q_1; \kappa, q_2)$ is not zero then, for the specified q_2 , the chosen κ is in a stopping band.

4.2. Results

The case $q_2 = 0$ will be considered in some detail. This case can be interpreted by writing the potential in terms of parts that are symmetric and antisymmetric in y so that

$$\phi(x, y) = \phi_S(x, y) + \phi_A(x, y), \quad (38)$$

where

$$\phi_S(x, y) = \frac{1}{2} [\phi(x, y) + \phi(x, -y)] \quad (39)$$

and

$$\phi_A(x, y) = \frac{1}{2} [\phi(x, y) - \phi(x, -y)], \quad (40)$$

and hence

$$\frac{\partial \phi_S}{\partial y}(x, 0) = \phi_A(x, 0) = 0. \quad (41)$$

From the Bloch conditions (14), it follows immediately that

$$\phi_S(x, W/2) = \frac{1}{2} [1 + e^{-iq_2 W}] \phi(x, W/2), \quad (42)$$

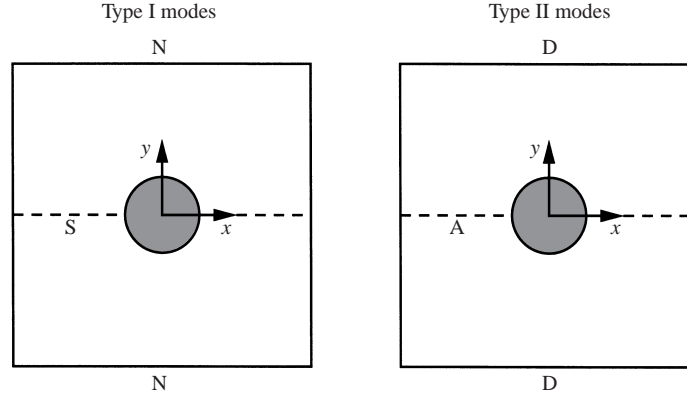


FIGURE 2. Boundary conditions and symmetries for type I and type II modes ($q_2 = 0$).
Notation: N–Neumann, D–Dirichlet, S–symmetric, A–antisymmetric.

$$\frac{\partial \phi_S}{\partial y}(x, W/2) = \frac{1}{2}[1 - e^{-iq_2 W}] \frac{\partial \phi}{\partial y}(x, W/2), \quad (43)$$

$$\phi_A(x, W/2) = \frac{1}{2}[1 - e^{-iq_2 W}] \phi(x, W/2), \quad (44)$$

$$\frac{\partial \phi_A}{\partial y}(x, W/2) = \frac{1}{2}[1 + e^{-iq_2 W}] \frac{\partial \phi}{\partial y}(x, W/2), \quad (45)$$

and so when $q_2 = 0$

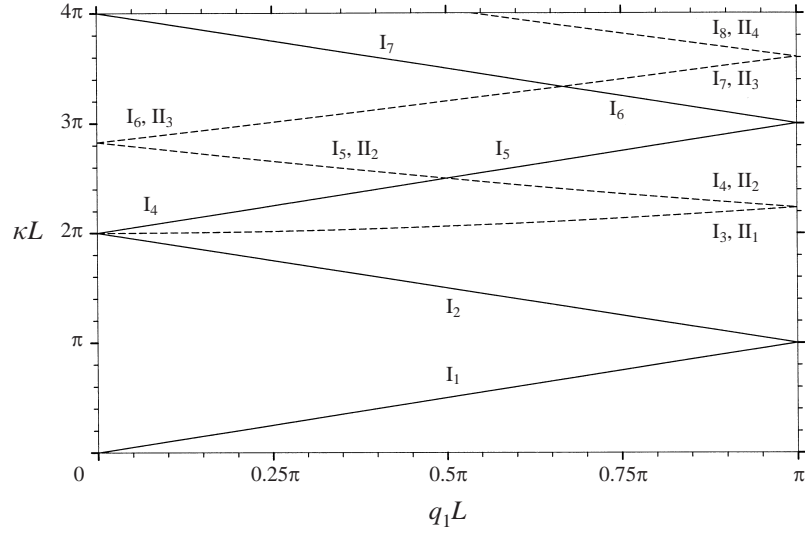
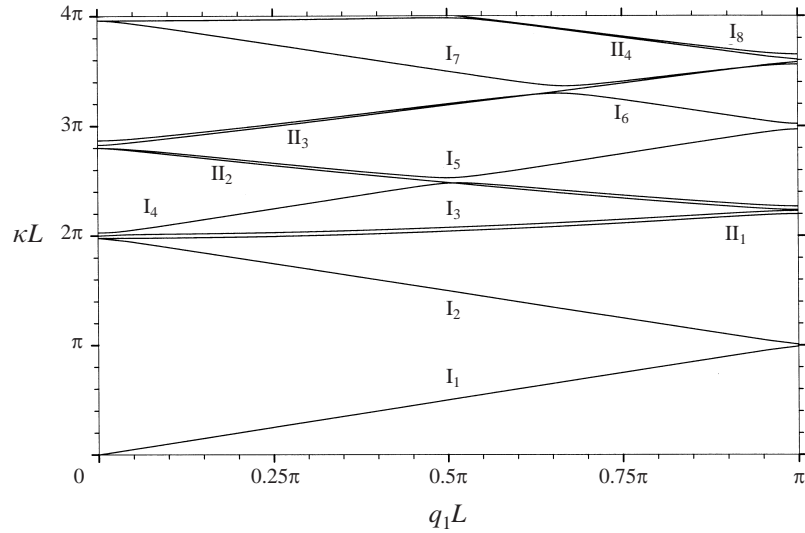
$$\frac{\partial \phi_S}{\partial y}(x, W/2) = \frac{\partial \phi_S}{\partial y}(x, -W/2) = \phi_A(x, W/2) = \phi_A(x, -W/2) = 0. \quad (46)$$

Thus, solutions to the problem with $q_2 = 0$ correspond either to motions that are symmetric about $y = 0$ and satisfy homogeneous Neumann conditions on $y = \pm W/2$ (referred to here as type I modes), or to solutions that are antisymmetric about $y = 0$ and satisfy homogeneous Dirichlet conditions on $y = \pm W/2$ (type II modes). The various boundary and symmetry conditions are illustrated in figure 2. All solutions satisfy the Bloch conditions (13).

The type I and type II modes (as well as other modes) could be solved for separately by making appropriate choices of trial function with trigonometric functions. However, the determination of the form of the elements of the matrices in (33) is then a rather longer calculation. It is simpler to adopt the approach given above and identify the modes by computing the boundary values of the eigenvector and its normal derivative.

Calculations are now presented for various geometrical parameters in figures 3–5; the results are displayed in the reduced-zone scheme discussed at the end of §2. Because of the geometrical symmetries, a reversal in the sign of q_1 gives essentially the same solution, but with wave propagation in the opposite direction, and thus attention is restricted to $q_1 L \in [0, \pi]$. Before presenting numerical results for the full problem, it is instructive to consider the problem when there is no cylinder present so that only the Bloch conditions need be satisfied. For simplicity, attention will be restricted to modes with $\kappa W < 4\pi$; for any q_1 , type I modes are

$$\phi = e^{iq_1 x}, \quad \kappa = q_1, \quad (47)$$

FIGURE 3. Eigenvalue κL vs. wave vector $q_1 L$; $W/L = 1$, $D/L = 0$, $q_2 L = 0$.FIGURE 4. Eigenvalue κL vs. wave vector $q_1 L$; $W/L = 1$, $D/L = 0.1$, $q_2 L = 0$.

$$\phi = e^{iq_1 x} \cos \frac{2\pi y}{W}, \quad \kappa = \left(q_1^2 + \frac{4\pi^2}{W^2} \right)^{1/2}, \quad (48)$$

and the only type II modes are

$$\phi = e^{iq_1 x} \sin \frac{2\pi y}{W}, \quad \kappa = \left(q_1^2 + \frac{4\pi^2}{W^2} \right)^{1/2}. \quad (49)$$

Clearly, the second type I mode and the type II mode share the same eigenvalue κ . Results for the case $W = L$ are displayed in figure 3 and each continuous curve linking $q_1 L = 0$ to $q_1 L = \pi$, here called a branch, is labelled as either type I or type II. The branches of each mode type are indexed in strictly ascending order of κL .

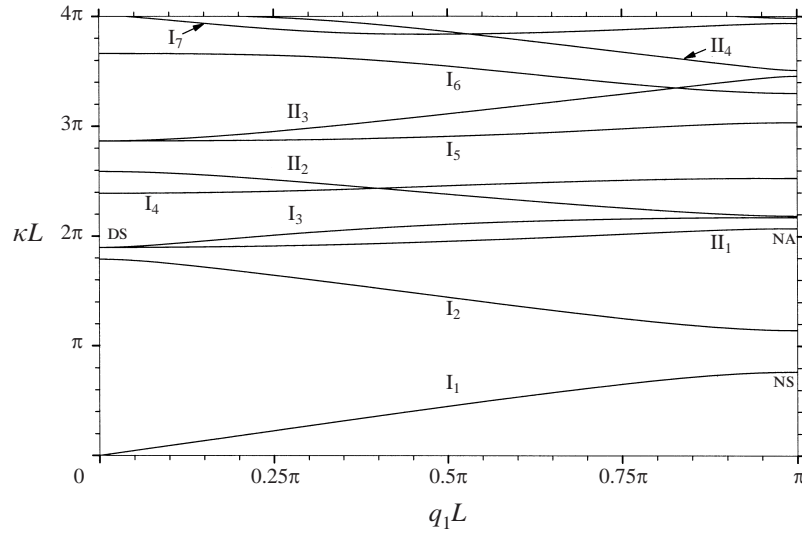


FIGURE 5. Eigenvalue κL vs. wave vector $q_1 L$; $W/L = 1$, $D/L = 0.5$, $q_2 L = 0$.

Note that some branches of type I modes cross and the indexing has been chosen to reflect the behaviour observed when a cylinder is introduced.

For a cylinder of non-zero but small radius, as in figure 4, the pattern is superficially very similar. However, there are three significant differences. First, the type I and type II modes with identical eigenvalues in the absence of the cylinder have now split; identification of the branches was made by computing the corresponding eigenvector and verifying the boundary conditions. Secondly, the crossings of type I modes no longer exist. This has been verified carefully by increasing the accuracy of the computations in these regions. Finally, with non-zero D/L there are so-called band gaps, although this is not immediately apparent from figure 4 as they are quite narrow. For example, for $0.99\pi \lesssim \kappa L \lesssim 1.01\pi$ there is no corresponding real value of $q_1 L$. In other words, for κL in this range (and for $q_2 L = 0$) it is not possible for waves to propagate through the array without change of amplitude.

For a larger radius, as in figure 5, the situation is more confused and it is not easy to identify the different modes by direct comparison with figure 3. The labelling on the figure was arrived at by observing the changes as D/L was increased through values not displayed here, and confirmed by computation of the eigenvector. The existence of band gaps is now clearly displayed; the first band gap has now widened to $0.77\pi \lesssim \kappa L \lesssim 1.14\pi$. The significance of these band gaps will be discussed later in §§ 6–7.

For $q_1 L$ equal to either zero or π , the solutions obtained may satisfy either homogeneous Dirichlet or homogeneous Neumann conditions on $x = \pm L/2$. This can be seen explicitly by examining the symmetries of ϕ as in equations (42)–(45). In particular, $q_1 L = 0$ can correspond to either the symmetric Neumann modes or the antisymmetric Dirichlet modes while $q_1 L = \pi$ can correspond to either the antisymmetric Neumann or the symmetric Dirichlet modes. Similar comments apply to $q_2 W$ and the cell boundaries at $y = \pm W/2$. Hence, for $q_1 L$ and $q_2 W$ both equal to one of zero or π , the solutions obtained may correspond to standing waves satisfying the same homogeneous boundary condition on opposite sides of the cell. To obtain other standing-wave solutions satisfying, for example, a homogeneous Neumann

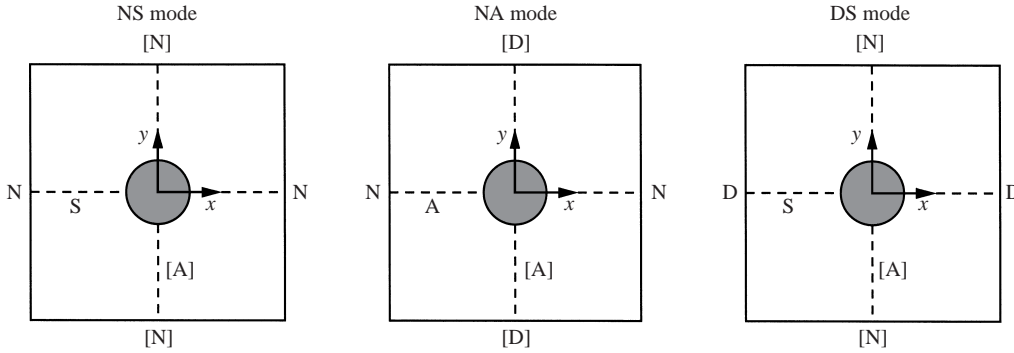


FIGURE 6. Boundary conditions and symmetries for NS, NA and DS modes ($q_2 = 0$).
Notation: N–Neumann, D–Dirichlet, S–symmetric, A–antisymmetric.

condition on $x = -L/2$ and a homogeneous Dirichlet condition on $x = L/2$ the underlying periodicity of the solutions must be increased to accommodate a cell of twice the size.

4.3. Connection with trapped modes

The variational method is now used to investigate how so-called ‘trapped modes’ are recovered as one of the cell dimensions, W say, is allowed to increase indefinitely. A trapped mode is a free oscillation of finite energy within an unbounded fluid. Callan, Linton & Evans (1991) proved that such trapped modes may exist within a rigid, parallel-walled channel of infinite length that has a rigid cylinder symmetrically placed about the centreline. Subsequently, trapped modes have been found to exist when homogeneous Dirichlet conditions are applied on the channel walls (this is non-physical within the context of water waves in a channel, but the problem can be interpreted in terms of wave interaction with arrays of cylinders; see Maniar & Newman 1997).

Evans & Porter (1999) give a review of the present state of knowledge regarding trapped modes supported by a rigid cylinder in a channel, and the following summarizes some of these results using their notation for mode identification (the notation is illustrated in figure 6). Modes satisfying Neumann (Dirichlet) conditions on the channel walls, here $x = \pm L/2$, are denoted by N(D) and modes that are symmetric (antisymmetric) about $y = 0$ are denoted by S(A). For some $\kappa L \in (0, \pi)$ an NS trapped mode exists for any D/L , but an NA mode exists only for $D/L \gtrsim 0.81$. For some $\kappa L \in (0, 2\pi)$ a DS mode exists for all $D/L \lesssim 0.68$, but no corresponding DA mode has been found. All of these modes are antisymmetric about the centreline of the channel $x = 0$ and are below the first appropriate cut-off frequency for antisymmetric propagating modes. The cut-off for Neumann modes is $\kappa L = \pi$ and for Dirichlet modes it is $\kappa L = 2\pi$.

The notation described above has been used to identify some of the standing-wave modes in figure 5. In view of equations (42)–(45), for the Bloch problem this notation is sufficient to identify all boundary conditions applied on the cell perimeter and all symmetries about $x = 0$ and $y = 0$; see figure 6. In this figure, the letters not in square brackets correspond to the boundary conditions and symmetries associated directly with the mode name. For $q_1 L = 0$ there is a double eigenvalue at $\kappa L \simeq 1.896\pi$ and the DS mode is the limit of the I_3 curve as $q_1 L \rightarrow 0$. Data showing the approach to trapped modes as W/L increases are given in table 1. The trapped mode frequencies

W/L	κL (0.5, NS)	κL (0.9, NS)	κL (0.9, NA)	κL (0.5, DS)
1	0.765π	0.526π	2.053π	1.896π
2	0.860π	0.818π	1.149π	1.942π
3	0.879π	0.851π	1.031π	1.951π
4	0.884π	0.859π	1.002π	1.954π
5	0.885π	0.860π	0.992π	1.955π
∞	0.886π	0.861π	0.99π	1.956π

TABLE 1. Approach of standing-wave frequencies to trapped-mode frequencies as the cell aspect ratio $W/L \rightarrow \infty$. The number in parentheses is the cylinder diameter D/L and the letters identify the mode (see the text and figures 5 and 6).

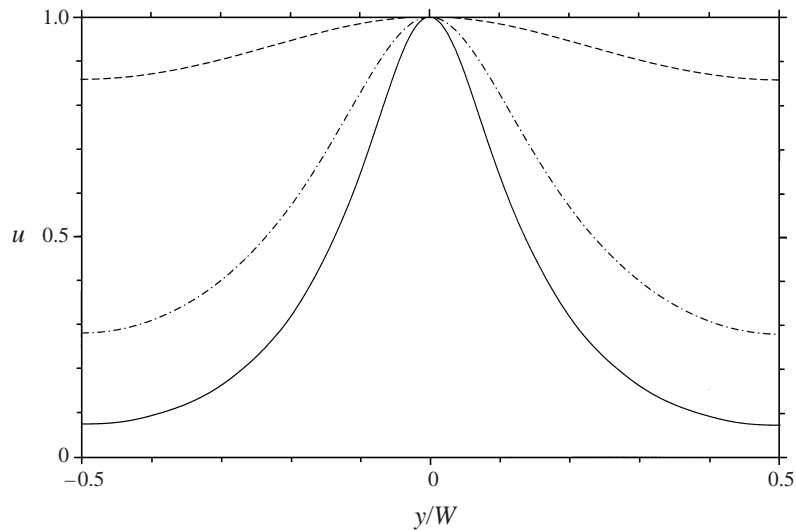


FIGURE 7. Approximate eigenfunction u (NS mode) vs. y/W on $x = L/2$ for $W/L = 1$ (---), $W/L = 3$ (-·-·-), and $W/L = 5$ (—); $D/L = 0.5$, $q_2L = 0$.

($W/L \rightarrow \infty$) are taken from Maniar & Newman (1997) for the NS and DS modes, and from Evans & Porter (1999) for the NA mode. The latter value was estimated from graphical results and so is given to only two significant figures.

Consider first the modes corresponding to $q_1L = \pi$. For $D/L = 0.5$, as $W/L \rightarrow \infty$ the NS mode marked in figure 5 remains the only mode below $\kappa L = \pi$. All other modes remain above $\kappa L = \pi$, and will tend asymptotically to a cut-off at $\kappa L = n\pi$ for some positive integer n (under the assumption that there are no ‘embedded’ trapped modes for this geometry, that is trapped modes with wavenumbers above the cut off at $\kappa L = \pi$). For this NS mode, the convergence of κL to the trapped mode value as W/L increases is shown in table 1. For $D/L = 0.5$, the marked NA mode does not become a trapped mode. However, for $D/L = 0.9$, as $W/L \rightarrow \infty$ the lowest NS and NA modes both asymptote to trapped modes below the cut-off at $\kappa L = \pi$ as shown in table 1. Again, all other modes appear to remain above the cut-off as W/L is increased.

The eigenvalues are clearly very close to the trapped-mode frequencies for $W/L = 5$. The change in the approximate eigenfunction u (calculated from equation (31)) as W/L increases is illustrated in figure 7 for an NS mode showing that, as $W/L \rightarrow \infty$,

q_1L	$\frac{1}{5}\pi$	$\frac{1}{4}\pi$	$\frac{1}{3}\pi$	$\frac{2}{5}\pi$	$\frac{1}{2}\pi$	$\frac{3}{5}\pi$	$\frac{2}{3}\pi$	$\frac{3}{4}\pi$	$\frac{4}{5}\pi$
κL (BB)	0.197π	0.246π	0.328π	0.394π	0.491π	0.588π	0.651π	0.728π	0.773π
κL (RB)	0.200π	0.250π	0.332π	0.398π	0.497π	0.594π	0.657π	0.733π	0.777π

TABLE 2. Comparison between the present calculations (BB) and Rayleigh–Bloch wave frequencies (RB); $W/L = 5$, $D/L = 0.5$, $q_2L = 0$.

u becomes increasingly concentrated around $y = 0$ and seems to approach zero at $y/W = \pm\frac{1}{2}$, which is the expected behaviour if the limit is to be a trapped mode.

The final mode marked in figure 5 is the DS mode corresponding to $q_1L = 0$. The antisymmetric propagating-wave cut-off is at $\kappa L = 2\pi$ when Dirichlet conditions are applied on the channel walls and the trapped mode value of κL is now a little below 2π (see table 1). As W/L is increased, more and more modes move below $\kappa L = 2\pi$. Calculations suggest that, with the exception of the DS mode, these modes all satisfy Neumann conditions on $x = \pm L/2$ and are symmetric about $x = 0$; in an infinite channel there is no positive cut-off frequency for such modes and so in general the potential will not decay to zero as $|y| \rightarrow \infty$. Thus, it seems that the single DS mode is the only mode that can asymptote to a trapped mode for $q_1L = 0$ and $\kappa L < 2\pi$.

Note that standing waves that asymptote to trapped modes can be found irrespective of whether a Dirichlet or Neumann boundary condition is applied on $y = \pm W/2$ (that is whether $q_2W = 0$ or $q_2W = \pi$ respectively). In fact, for $\kappa L < \pi$ the standing-wave frequency obtained from the Dirichlet conditions provides an upper bound for the trapped-mode frequency and that from the Neumann problem provides a lower bound; this result has been established for trapped modes by Khallaf, Parnovski & Vassiliev (2000, § 3).

4.4. Connection with Rayleigh–Bloch waves

A generalization of a trapped mode is the so-called ‘Rayleigh–Bloch’ wave. Such waves may propagate along an infinite row of equally spaced, rigid, vertical cylinders with decay of the fluid motion to zero in the direction normal to the row. Evans & Porter (1999) give a review of the present state of knowledge concerning Rayleigh–Bloch waves of this type and they report two types of such waves that, for a fixed $q_1L \leq \pi$, exist for discrete $\kappa L \in (0, q_1L)$. These are waves symmetric about $x = 0$ that exist for all non-dimensional cylinder diameters $D/L \in (0, 1]$, and waves antisymmetric about $x = 0$ that exist only when $0.81 \lesssim D/L \leq 1$. As for trapped modes, the numerical evidence suggests that the frequencies of Rayleigh–Bloch waves are recovered in the present problem by taking the limit $W/L \rightarrow \infty$. Comparison between the present calculations and those for symmetric Rayleigh–Bloch waves made by Porter & Evans (1999, table 2) is made in table 2.

Another example is illustrated in figure 8. For $D/L = 0.9$, all but two of the frequency curves remain above the cut-off at $\kappa L = q_1L$. The complete curve below the cut-off corresponds to symmetric Rayleigh–Bloch waves and the partial curve to antisymmetric Rayleigh–Bloch waves. The latter curve is close to the appropriate curve in figure 10(b) of Evans & Porter (1999). Calculations for $D/L = 0.5$ are reported by Evans & Porter (1999) and McIver, Linton & McIver (1998) and their graphical results may be compared with the I_1 curve in the present figure 5.

The limiting values as $q_1L \rightarrow \pi$ of the Rayleigh–Bloch wavenumbers κL corresponding to the two lowest curves in figure 8 are just the NS and NA trapped

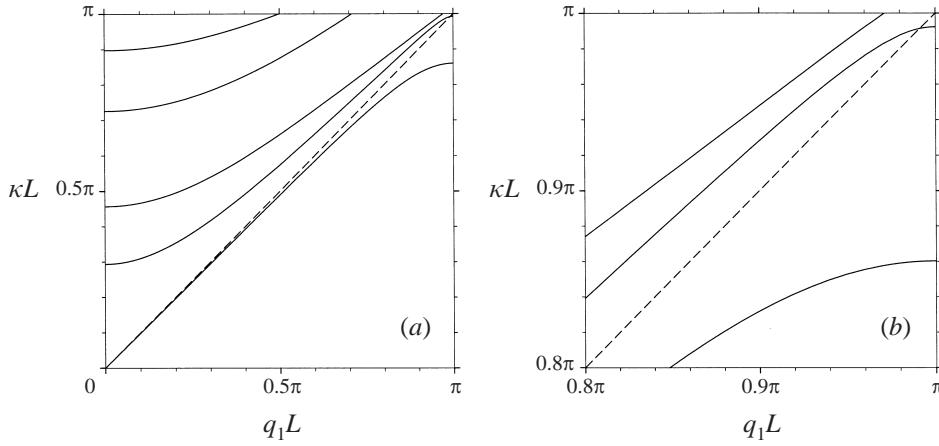


FIGURE 8. (a) Eigenvalue κL vs. wave vector $q_1 L$; $W/L = 5$, $D/L = 0.9$, $q_2 L = 0$. (b) An enlargement of part of (a). The dashed line is the cut-off $\kappa L = q_1 L$.

modes for $D/L = 0.9$ given in table 1. All known Rayleigh–Bloch waves become trapped waves in this limit. The DS mode discussed in §4.3 is not the limit of any known Rayleigh–Bloch wave and it may be that there is a hitherto undiscovered Rayleigh–Bloch wave for which the DS mode is the limit.

5. Numerical calculations within the stopping bands

The variational method of §4 is suitable only for calculations within passing bands, that is when the Bloch wave vector $\mathbf{q} = \{q_1, q_2\}$ is real. In this section an outline is given of two standard numerical methods that can be used for calculations within stopping bands when, in general, \mathbf{q} is complex and the amplitude of a wave will decay as it propagates. Like the method of §4, no assumptions are made about the parameter sizes or the direction of propagation and so these techniques are both more accurate and more general than the wide-spacing approximation of §3.

5.1. Point-matching formulation

For specified κ and q_2 , the problem defined by equations (2) and (13)–(15) may be formulated as an eigenvalue problem for q_1 as follows. The series

$$\phi = A_0 C_0(\kappa r) + \sum_{n=1}^N C_n(\kappa r) (A_n \cos n\theta + B_n \sin n\theta), \quad (50)$$

where

$$C_n(\kappa r) = J_n(\kappa r) Y_n'(\kappa D/2) - Y_n(\kappa r) J_n'(\kappa D/2), \quad (51)$$

satisfies both the field equation (2) and the cylinder boundary condition (15). Here J_n and Y_n denote Bessel functions of order n . The remaining Bloch conditions (13)–(14) are satisfied pointwise. Let $(r, \theta) = (r_i, \theta_i)$ be the polar coordinates of $P + Q$ points on two sides of the primitive cell $\{|x| \leq L/2, |y| \leq W/2\}$. The first P points are on $\{x = L/2, |y| \leq W/2\}$ and, in order to apply the Bloch conditions, complementary points $(r, \theta) = (r_i, \pi - \theta_i)$ are required on $\{x = -L/2, |y| \leq W/2\}$. The remaining Q points are on $\{y = W/2, |x| \leq L/2\}$ with complementary points $(r, \theta) = (r_i, -\theta_i)$ on $\{y = -W/2, |x| \leq L/2\}$.

Application of the Bloch conditions at these points leads to a system of equations for the unknown coefficients $\{A_0, A_1, \dots, A_N, B_1, \dots, B_N\} = \mathbf{x}^T$, say. If the conditions are satisfied in the least-squares sense then a necessary condition for a minimum of the sum of squares of the residuals with respect to \mathbf{x} has the form

$$\mathbf{A}\mathbf{x} = \mathbf{0}, \quad (52)$$

where \mathbf{A} is a $(2N+1) \times (2N+1)$ matrix. There is a non-trivial solution for \mathbf{x} provided $\det \mathbf{A} = 0$. Rather than seek a zero of $\det \mathbf{A}$, values of κL and $q_2 W$ are specified and $|\det \mathbf{A}|$ minimized as a function of $q_1 L$. This formulation works very well for $\kappa W \lesssim 2\pi$. Within this range, an accuracy for $q_1 L$ of a three digits or more is usually obtained for $N = 16$ and $P = Q = 4N$.

The system of equations resulting from application of the Bloch conditions may also be rewritten as a generalized eigenvalue problem for the eigenvalue $e^{iq_1 L}$ which can be solved using the QZ algorithm (Golub & Van Loan 1983). A reduction to a standard eigenvalue problem is not possible in general as the matrices involved become nearly singular as P and Q are increased. The method works well for $\kappa L \lesssim 4\pi$, but for $\kappa L \gtrsim 4\pi$ large values of N , P and Q are required to obtain reasonable accuracy and the QZ algorithm becomes unreliable and may converge to erroneous values if insufficient care is taken. With this in mind a more robust, but more expensive, method of computation is described in the next section.

5.2. Boundary-integral formulation

For given κ and q_2 , the problem defined by equations (2) and (13)–(15) may be formulated as an eigenvalue problem for q_1 using an application of Green's theorem to the potential ϕ and a suitable Green's function G . The Green's function is chosen to satisfy the cylinder-surface boundary condition (15) and is

$$G(x, y; \xi, \eta) = H_0(\kappa R) - \sum_{n=0}^{\infty} \epsilon_n \frac{J'_n(\kappa D/2)}{H'_n(\kappa D/2)} H_n(\kappa \rho) H_n(\kappa r) \cos n(\theta - \psi). \quad (53)$$

Here, (ρ, ψ) and (ξ, η) are respectively the polar and Cartesian coordinates of the source point P , (r, θ) and (x, y) are the corresponding coordinates of the field point Q , R is the distance between P and Q and satisfies

$$R^2 = (x - \xi)^2 + (y - \eta)^2 = r^2 + \rho^2 - 2r\rho \cos(\theta - \psi), \quad (54)$$

H_n denotes the Hankel function of the first kind and order n , $\epsilon_0 = 1$, and $\epsilon_n = 2$ for $n \geq 1$. That G satisfies the boundary condition (15) may be verified using Graf's addition theorem (Abramowitz & Stegun 1964, equation 9.1.79).

With the above choice of Green's function, Green's theorem yields

$$\phi(P) = \frac{1}{2i} \int_S \left(\phi(Q) \frac{\partial G}{\partial n_Q}(P; Q) - G(P; Q) \frac{\partial \phi}{\partial n_Q}(Q) \right) ds_Q \quad (55)$$

where the integration is taken over the boundary S of the rectangular region $\{|x| \leq L/2, |y| \leq W/2\}$, and the subscript Q on the outward normal coordinate n and the tangential coordinate s is used to denote derivatives with respect to the field variables. Substitution of the representation (55) into the conditions on ϕ in equations (13)–(14), and application of all of (13)–(14) under the integral sign, gives a set of four coupled integral equations for the four unknown functions:

$$f(y) \equiv \phi(L/2, y), \quad u(y) \equiv \frac{\partial \phi}{\partial x}(L/2, y), \quad |y| \leq W/2, \quad (56)$$

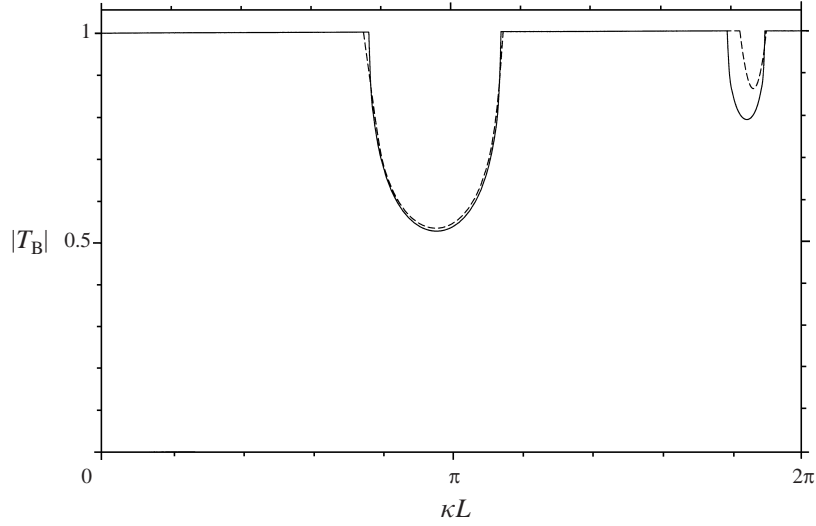


FIGURE 9. Bloch transmission coefficient $|T_B|$ vs. wavenumber κL ; $W/L = 1$, $D/L = 0.5$, $q_2 L = 0$: —, full numerical calculations; - - -, solutions of equation (29).

$$g(x) \equiv \phi(x, W/2), \quad v(x) \equiv \frac{\partial \phi}{\partial y}(x, W/2), \quad |x| \leq L/2. \quad (57)$$

Divide the interval $|y| \leq W/2$ into M elements of equal length and the interval $|x| \leq L/2$ into N elements of equal length. The functions $f(y)$, $u(y)$, $g(x)$ and $v(x)$ are assumed to be constant over the appropriate individual elements which allows the simultaneous integral equations to be reduced in a standard way to a matrix system for the unknown function values that has the form

$$\mathbf{A}(\lambda_2, \kappa L)\mathbf{x} = \lambda_1 \mathbf{B}(\lambda_2, \kappa L)\mathbf{x}, \quad (58)$$

where $\lambda_1 = e^{iq_1 L}$, $\lambda_2 = e^{iq_2 W}$, \mathbf{A} and \mathbf{B} are matrices of order $2(N+M) \times 2(N+M)$, and \mathbf{x} is the vector of unknown function values. Equation (58) is a generalized eigenvalue problem for the eigenvalue λ_1 which can be solved by the QZ algorithm (Golub & Van Loan 1983). Significant reduction in computational time can be obtained by reducing the size of the system by elimination from (58) of the elements of \mathbf{x} that correspond to values of $f(y)$ and $u(y)$. Note that a reduction to a standard eigenvalue problem is not possible as the matrices involved become nearly singular as M and N increase. Computations for a square cell suggest that $q_1 L$ may be computed to about three-figure accuracy for $\kappa L \lesssim 4\pi$ by taking $M = N = 16$. The boundary-integral method is recommended for calculations of T_B in the stopping bands for $\kappa L \gtrsim 2\pi$.

5.3. Results

Here results are presented that were obtained using the methods of §5.1 and §5.2. Typical results for the Bloch transmission coefficient $T_B = e^{iq_1 L}$ (see §3) are illustrated in figure 9 for the case $q_2 L = 0$. As noted previously, because of the geometrical symmetries, a reversal in the sign of q_1 gives essentially the same solution, but with wave propagation in the opposite direction, and thus attention is restricted to $\text{Re } q_1 L \in [0, \pi]$. The parameter values used are the same as in figure 5 in which the passing and stopping bands may be identified and compared with the results shown in figure 9. The ranges $0 < \kappa L \lesssim 0.77\pi$, $1.14\pi \lesssim \kappa L \lesssim 1.79\pi$ and $1.90\pi \lesssim \kappa L < 2\pi$ are passing bands where $|T_B| = 1$ so that the waves propagate through the

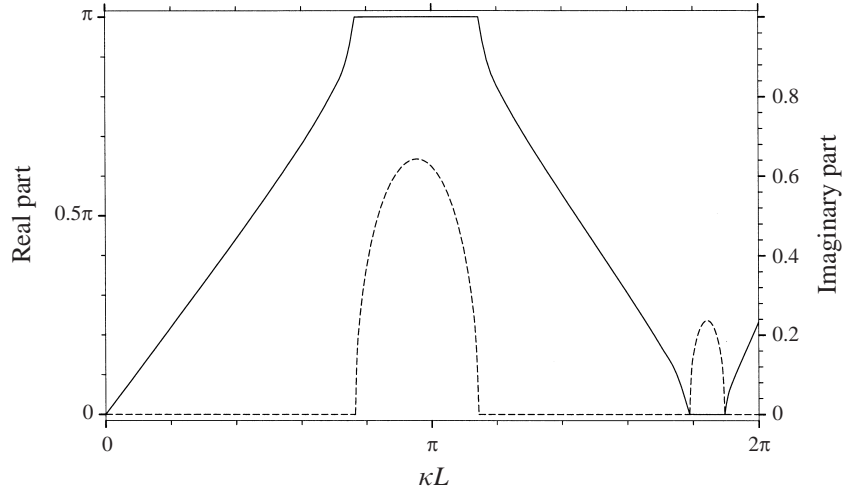


FIGURE 10. Real (—) and imaginary (---) parts of q_1L vs. wavenumber κL ; $W/L = 1$, $D/L = 0.5$, $q_2L = 0$.

array with constant amplitude. The complementary ranges $0.77\pi \lesssim \kappa L \lesssim 1.14\pi$ and $1.79\pi \lesssim \kappa L \lesssim 1.90\pi$ are stopping bands in which $|T_B| < 1$ so that the waves change in amplitude as they propagate. In the full numerical calculations of figure 9 the passing bands were first identified using the method of §4.1 and then T_B was computed in the stopping bands using the above least-squares formulation. Comparison is made with the wide-spacing approximation result (29) and the agreement is generally excellent despite the violation of the assumptions behind the approximation. The reduction in the accuracy near $\kappa W = 2n\pi$, where n is a positive integer, is typical; this point is discussed further in §7.

Figure 10 shows how the real and imaginary parts of q_1L vary with κL for the same geometry as used in figure 9. The solutions displayed have positive imaginary part; there are corresponding solutions with negative imaginary parts of equal magnitude. As κL is increased in the first passing band, $\text{Im}\{q_1L\} = 0$ and the I_1 mode is followed up to the first stopping band. Within the stopping band the phase $\text{Re}\{q_1L\}$ remains constant while $\text{Im}\{q_1L\}$ varies. The I_2 mode is then followed until the second stopping band where $\text{Re}\{q_1L\}$ again remains constant. After the second stopping band there are two modes; the II_1 mode is followed in figure 10. The qualitative behaviour obtained here from numerical calculations confirms exactly that observed in the approximate solution of §3 that is based upon a wide-spacing approximation.

6. Unidirectional wave propagation through an array

The behaviour described in the preceding sections for a doubly infinite array is related to the reflection and transmission properties of an array that has finite length in the x -direction. In particular, for wave parameters that correspond to the stopping bands of the infinite array problem, there is little transmission through a finite array even when there is only a small number of rows. This is illustrated here for normal incidence, $q_2 = 0$, and $\kappa W < 2\pi$ using the wide-spacing formalism of Evans (1990). This is based on the same assumptions made in the approximate calculation of the Bloch transmission coefficient described in §3. Consider N infinitely long rows of cylinders situated at $x = L_m$, $m = 1, 2, \dots, N$. Each row may be thought of as a single

cylinder with axis on $y = 0$ between channel walls at $y = \pm W/2$. Divide the fluid domain into $N + 1$ regions as follows:

$$\left. \begin{array}{l} \text{Region 1:} \quad -\infty < x < L_1, \\ \text{Region } m: \quad L_{m-1} < x < L_m, \quad m = 2, 3, \dots, N, \\ \text{Region } N + 1: \quad L_N < x < \infty. \end{array} \right\} \quad (59)$$

Here $L_{m+1} - L_m = L$, $m = 1, 2, \dots, N - 1$. It will be assumed that $\kappa L \gg 1$. Suppose that an incident plane wave propagates in the direction of x increasing and this is reflected and transmitted by the complete grating. Under the wide-spacing approximation, at sufficiently large distances from the cylinders, in region m the solution may be written as

$$\phi = A_m e^{i\kappa x} + B_m e^{-i\kappa x}. \quad (60)$$

In region 1 this will correspond to the incident and reflected wave for the complete grating and in region $N + 1$ to the transmitted wave. The solutions in region m and region $m + 1$ may be related to the reflection and transmission coefficients for a single row, R and T respectively, in the same way as described before equations (20). This leads to the equations

$$A_1 = 1, \quad B_1 = R_N, \quad A_{N+1} = T_N, \quad B_{N+1} = 0, \quad (61)$$

$$\left. \begin{array}{l} A_{m+1} e^{i\kappa L_m} = T A_m e^{i\kappa L_m} + R B_{m+1} e^{-i\kappa L_m}, \\ B_m e^{-i\kappa L_m} = T B_{m+1} e^{-i\kappa L_m} + R A_m e^{i\kappa L_m}, \end{array} \right\} \quad m = 1, 2, \dots, N, \quad (62)$$

where R_N and T_N are the reflection and transmission coefficients for the complete array of N rows. The steps described by Evans (1990) allow this system to be rewritten in the form

$$\begin{pmatrix} T_N e^{i(\kappa L_N + \kappa L)} \\ 0 \end{pmatrix} = \mathbf{S}^N \begin{pmatrix} e^{i\kappa L_1} \\ R_N e^{-i\kappa L_1} \end{pmatrix} \quad (63)$$

where \mathbf{S} is the scattering matrix defined in equation (23). The system is easily solved to determine R_N and T_N . Let

$$\mathbf{S}^N \equiv \begin{pmatrix} s_{11} & s_{12} \\ s_{21} & s_{22} \end{pmatrix} \quad (64)$$

then, in particular,

$$T_N = e^{i\kappa(L_1 - L_N - L)} \left(s_{11} - \frac{s_{12}s_{21}}{s_{22}} \right). \quad (65)$$

For purely numerical purposes it is straightforward to evaluate \mathbf{S}^N directly. However, Evans (1990) gives an explicit formula for \mathbf{S}^N which yields further insight into the problem. From Evans' result it is easy to deduce that

$$s_{11} - \frac{s_{12}s_{21}}{s_{22}} = \frac{\sinh \beta}{\sinh(\beta - N\alpha)} \quad (66)$$

where

$$\cosh \alpha = \frac{e^{i\kappa L}}{2T} (T^2 - R^2 + e^{-2i\kappa L}) = \frac{\cos(\delta + \kappa L)}{|T|}, \quad (67)$$

$$\cosh \beta = \frac{e^{i\kappa L}}{2R} (T^2 - R^2 - e^{-2i\kappa L}) = \frac{\sin(\delta + \kappa L)}{|R|}, \quad (68)$$

and δ is the phase of the transmission coefficient introduced in equation (25). From

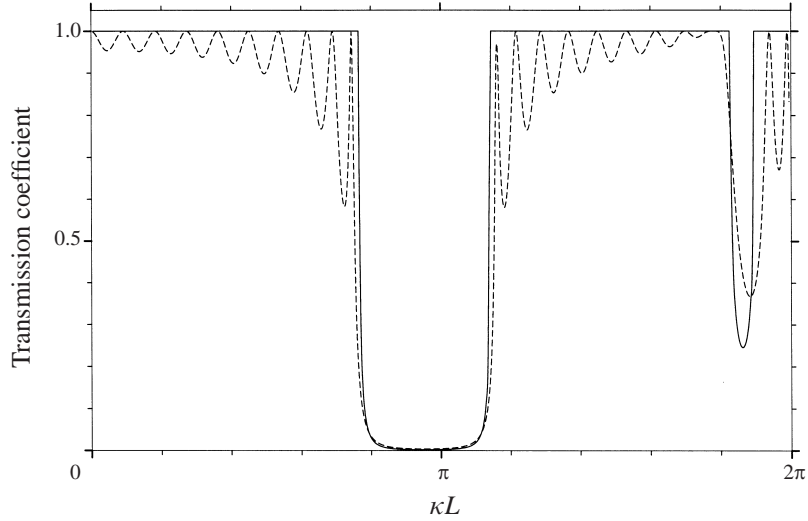


FIGURE 11. Transmission coefficient $|T_{10}|$ for ten rows of cylinders (dashed line) and Bloch transmission coefficient $|T_B|^{10}$ (solid line) vs. wavenumber κL ; $W/L = 1$, $D/L = 0.5$.

equation (29) it may be seen that α is directly related to the Bloch wavenumber q_1 in the corresponding periodic-array problem.

At wave frequencies for which $|T| < |\cos(\delta + \kappa L)|$, α has a non-zero real part and β is pure imaginary. Let $\beta = ib$ so that

$$|T_N|^2 = \frac{\sin^2 b}{\sin^2 b + \sinh^2 N\alpha} \quad (69)$$

and it is readily apparent that $|T_N| \rightarrow 0$ as $N \rightarrow \infty$. The frequencies at which this behaviour occurs correspond precisely to the stopping bands in the infinite-array problem. At wave frequencies for which $|T| > |\cos(\delta + \kappa L)|$, $\alpha = iq_1 L$ is pure imaginary and $\cosh \beta$ and $\sinh \beta$ are both real. In this case

$$|T_N|^2 = \frac{\sinh^2 \beta}{\sinh^2 \beta + \sin^2 Nq_1 L}, \quad (70)$$

and hence $|T_N|$ is oscillatory. The frequencies at which this behaviour occurs correspond precisely to the passing bands in the infinite-array problem.

The above behaviour of T_N is confirmed in figure 11 using results for a grating with $N = 10$ rows. The required reflection and transmission coefficients for a single cylinder were calculated by the method of Linton & Evans (1993). Comparison is made with $|T_B|^{10}$ which is the transmission coefficient for propagation through a distance $10L$ in the doubly infinite array. The oscillatory behaviour in $|T_{10}|$ is due to end effects for the finite number of rows. Clearly, the Bloch transmission coefficient may be used to predict the properties of a large, but finite, number of rows of cylinders. Similar numerical comparisons of the Bloch transmission coefficient with the transmission by finite arrays have been made by Heckl & Mulholland (1995) in the context of acoustic transmission in tube bundles.

The approximate positions of the troughs in transmission (and hence peaks in reflection) can be explained through the phenomenon of Bragg scattering that is well-known in x-ray diffraction by a crystal (Ashcroft & Mermin 1976, p. 96). For strong

overall reflection to occur the waves reflected from different rows of a grating must interfere constructively and, for the normal incidence investigated here, this occurs when $\kappa L = n\pi$, for integer n , which is clearly consistent with the results of figure 11.

7. Multi-directional wave propagation through an array

The previous section dealt with normal incidence on a grating and with frequencies where the reflected and transmitted waves are also normal to the grating. This section deals with an arbitrary angle of incidence and with the general case where the reflected and transmitted fields may contain components whose propagation direction is not parallel to the incident wave. Again, the reflection and transmission properties of the finite array are related to the stopping and passing bands for the infinite array.

Consider wave scattering by a grating of N identical rows of cylinders as described at the beginning of §6; the configuration is assumed to be symmetric about $x = 0$. A wave with potential

$$\phi_I = e^{i\kappa r \cos(\theta - \theta_q)} \quad (71)$$

is incident from the left at an angle θ_q to the x -axis, where (r, θ) are polar coordinates defined by $(x, y) = (r \cos \theta, r \sin \theta)$. This wave will be diffracted to obtain a reflected field

$$\phi \sim \sum_{p=-\mu}^{\nu} R_{qp} e^{-i\kappa r \cos(\theta + \theta_p)} \quad \text{as } x \rightarrow -\infty \quad (72)$$

and a transmitted field

$$\phi \sim \sum_{p=-\mu}^{\nu} T_{qp} e^{i\kappa r \cos(\theta - \theta_p)} \quad \text{as } x \rightarrow \infty, \quad (73)$$

where

$$\sin \theta_p = \sin \theta_q + \frac{2p\pi}{\kappa W}, \quad (74)$$

$$\mu = [(1 + \sin \theta_q)\kappa W / 2\pi], \quad \nu = [(1 - \sin \theta_q)\kappa W / 2\pi], \quad (75)$$

and $[\cdot]$ indicates that the integer part should be taken (see Twersky 1962). The far-field forms (72)–(73) are valid for any integer $q \in [-\mu, \nu]$. Conservation of energy requires that the components of the reflection and transmission matrices \mathbf{R} and \mathbf{T} satisfy

$$\sum_{p=-\mu}^{\nu} (|R_{qp}|^2 + |T_{qp}|^2) \cos \theta_p = \cos \theta_q \quad (76)$$

(Twersky 1962). An algorithm for the computation of approximations to the reflection and transmission matrices for multiple rows from the properties of a single row is given by Heckl & Mulholland (1995, §3.2), and their formulation was used for the calculations described below. The reflection and transmission matrices for a single row were calculated using the method of Linton & Evans (1993).

Heckl & Mulholland (1995) also give an approximate method for the calculation of the Bloch transmission coefficient. When compared with the present methods there is good agreement except in the vicinity of $\kappa W = 2n\pi$, for positive integer n , where there can be considerable disagreement. This disagreement can be accounted for by the neglect of evanescent modes in the method of Heckl & Mulholland (1995). In particular, the decay with distance of evanescent modes can be small near $\kappa W = 2n\pi$, and hence they may make a significant contribution to hydrodynamic interactions.

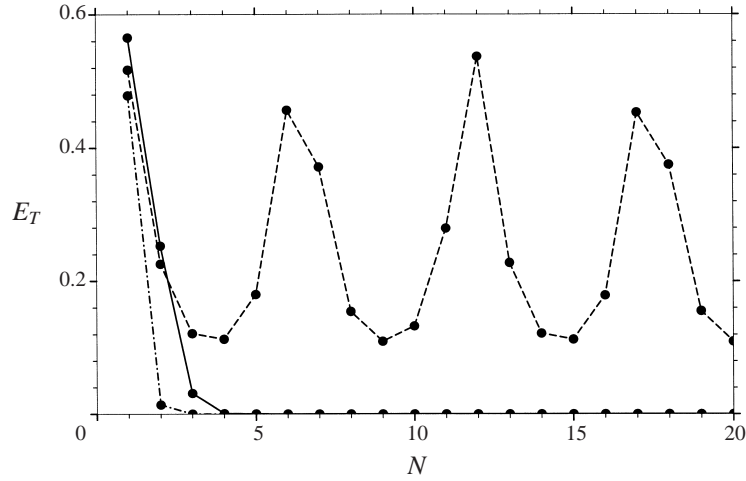


FIGURE 12. Transmitted energy E_T for normal wave incidence vs. number of rows of cylinders N ; $W/L = 1$, $D/L = 0.5$, $\kappa L = 2.7\pi$ ($-\cdot-\cdot-$), $\kappa L = 3\pi$ ($- - -$), $\kappa L = 3.7\pi$ ($—$).

Computations for scattering by multiple rows are now used to illustrate the relationship between that problem and the Bloch problem of wave transmission through an infinite array. The results in figure 12 are for normal incidence ($\theta_q = 0$) and show how the quantity

$$E_T = \sum_{p=-\mu}^{\nu} |T_{qp}|^2 \cos \theta_p, \quad (77)$$

which is proportional to the transmitted wave energy, varies with the number of rows N . Results are given for three wavenumbers $\kappa L \in (2\pi, 4\pi)$ for which, according to (75), there is a total of three propagating wave directions. The wavenumber $\kappa L = 2.7\pi$ is within a stopping band (see figure 5) and there is very little energy transmission through more than two rows of cylinders. By contrast, $\kappa L = 3\pi$ is within a passing band and there is significant wave transmission through any number of rows. The third value $\kappa L = 3.7\pi$ is not within a stopping band. However, it can be seen from figure 5 that the only mode that can propagate through an infinite array is antisymmetric about $y = 0$. However, under normal incidence, the scattering problem is completely symmetric and antisymmetric waves cannot be excited, leading to suppression of wave transmission through the finite array. If the angle of incidence is not zero but instead one of the other associated propagation directions, so that $\sin \theta_q = 2\pi/\kappa W$ say, then the problem is no longer completely symmetric and there is significant energy transmission through any number of rows for $\kappa L = 3.7\pi$. However, the transmission in the ‘symmetric’ normal direction is still negligible.

In this scattering problem, the complete solution has the form

$$\phi(x, y) = e^{iq_2 y} \psi(x, y), \quad (78)$$

where

$$q_2 = \kappa \sin \theta_q \quad (79)$$

and ψ is periodic in y with period W . Thus, the y variation is exactly that occurring in the Bloch problem. By specifying q_2 in the Bloch problem according to equation

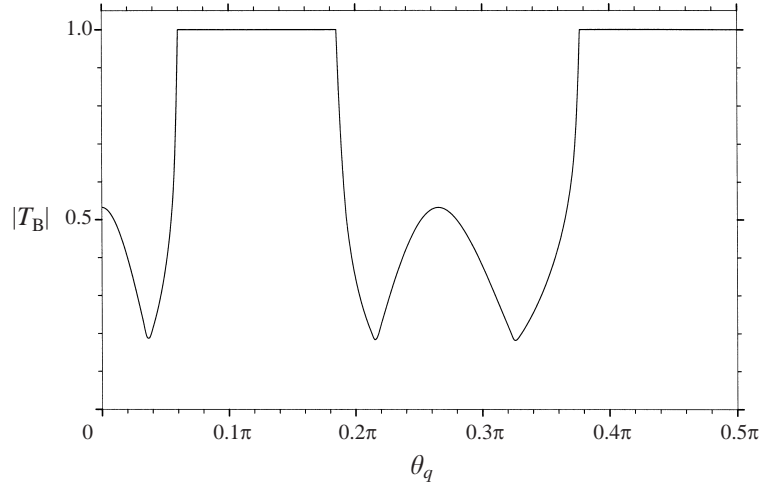


FIGURE 13. Maximum Bloch transmission $|T_B|$ vs. angle of incidence θ_q ; $W/L = 1$, $D/L = 0.5$, $\kappa L = 2.7\pi$.

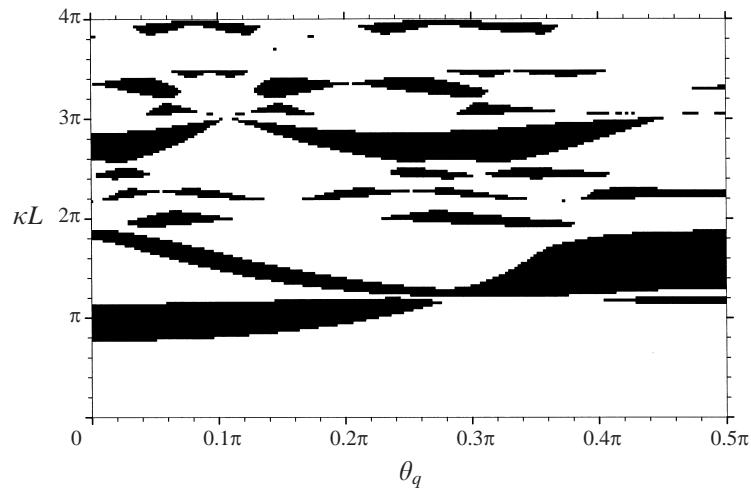


FIGURE 14. Passing (unshaded) and stopping (shaded) regions as a function of angle of incidence θ_q and wavenumber κL ; $W/L = 1$, $D/L = 0.5$.

(79) and solving for the Bloch transmission coefficient T_B useful information can be obtained about the scattering problem. For most wavenumbers there are at least two distinct values of $|T_B|$ and hence, in figure 13, the maximum $|T_B|$ is plotted as a function of angle for fixed κL . The variational method of §4.1 was used to identify the passing bands and the boundary-integral method of §5.2 was used to make calculations within the stopping bands. When $|T_B| = 1$ significant wave energy can be expected to propagate through a finite number of rows. When $|T_B| < 1$ little wave energy will propagate through the complete system and the decay with distance can be estimated from $|T_B|$.

A wider picture in figure 14 shows the distribution of passing and stopping regions as a function of incidence angle and wavenumber. This figure was constructed using the technique described at the end of §4.1. In the unshaded regions, $\max\{|T_B|\} = 1$

and in general there will be significant wave transmission through a finite array. In the shaded regions $|T_B| < 1$ and, in general, wave transmission will be effectively blocked within the first few rows of a finite array.

8. Conclusion

A variety of techniques has been presented for the calculation of water-wave propagation through an infinite array of vertical cylinders extending throughout the fluid depth and periodic in both horizontal directions. The phenomena of stopping and passing bands that arise in solid-state physics have been shown to arise in this water-wave Bloch problem as well.

The point-matching technique of § 5.1 may be extended to other cylinder geometries by modifying the series in equation (50). For example, the corresponding series for a circular cylinder extending through only part of the fluid depth can be calculated using the method given by Garrett (1971). For this geometry, the potential will no longer have the form (1). However, (1) will hold approximately sufficiently far from the cylinder for evanescent modes to be negligible, and so an approximate theory strictly valid only for small cylinder-to-spacing ratios is obtained. A similar modification of the Green's function (53) can be made in the boundary-integral method of § 5.2.

The final sections of the paper are devoted to the relationship between the Bloch problem and water-wave scattering by a finite number of rows, but where each row is of infinite extent. Further work is required to relate the Bloch problem to wave scattering by an array that is finite in both horizontal directions.

The author is grateful to Dr C. M. Linton for providing reflection and transmission data based on the work of Linton & Evans (1993), and to the referees for their suggestions that have significantly improved this paper.

REFERENCES

- ABRAMOWITZ, M. & STEGUN, I. A. 1964 *Handbook of Mathematical Functions*. National Bureau of Standards, Washington.
- ASHCROFT, N. W. & MERMIN, N. D. 1976 *Solid State Physics*. Saunders College, Philadelphia.
- CALLAN, M., LINTON, C. M. & EVANS, D. V. 1991 Trapped modes in two-dimensional wave guides. *J. Fluid Mech.* **229**, 51–64.
- CHIN, S. K., NICOROVICI, S. & MCPHEDRAN, R. C. 1994 Green's functions and lattice sums for electromagnetic scattering by a square array of cylinders. *Phys. Rev. E* **49**, 4590–4602.
- CHOU, T. 1998 Band structure of surface flexural-gravity waves along periodic interfaces. *J. Fluid Mech.* **369**, 333–350.
- DUFF, G. F. C. & NAYLOR, D. 1966 *Differential Equations of Applied Mathematics*. John Wiley & Sons.
- EVANS, D. V. 1990 The wide-spacing approximation applied to multiple scattering and sloshing problems. *J. Fluid Mech.* **210**, 647–658.
- EVANS, D. V. & PORTER, R. 1999 Trapping and near-trapping by arrays of cylinders in waves. *J. Enging Math.* **35**, 149–179.
- GARRETT, C. J. R. 1971 Wave forces on a circular dock. *J. Fluid Mech.* **46**, 129–139.
- GOLUB, G. H. & VAN LOAN, C. F. 1983 *Matrix Computations*. The Johns Hopkins University Press, Baltimore.
- HECKL, M. A. 1992 Sound propagation in bundles of periodically arranged cylindrical tubes. *Acustica*, **77**, 143–152.
- HECKL, M. A. & MULHOLLAND, L. S. 1995 Some recent developments in the theory of acoustic transmission in tube bundles. *J. Sound Vibr.* **179**, 37–62.
- KAGEMOTO, H. 1998 Wave decay characteristics along a long array of cylindrical legs. In *Proc. 13th*

- Intl Workshop on Water Waves and Floating Bodies, Alphen aan den Rijn, The Netherlands*, 55–58. Delft University of Technology, the Netherlands.
- KAGEMOTO, H. & YUE, D. K. P. 1986 Wave forces on a platform supported on a large number of floating legs. In *Proc. 5th Intl Conf. on Offshore Mechanics and Arctic Engineering*, vol. 1, pp. 206–211. ASME.
- KASHIWAGI, M. 2000 Wave interactions with a multitude of floating cylinders. In *Proc. 15th Intl Workshop on Water Waves and Floating Bodies, Caesarea, Israel*, pp. 99–102. Tel Aviv University, Israel.
- KHALLAF, N. S. A., PARNOVSKI, L. & VASSILIEV, D. 2000 Trapped modes in a waveguide with a long obstacle. *J. Fluid Mech.* **403**, 251–261.
- LINTON, C. M. & EVANS, D. V. 1993 The interaction of waves with a row of circular cylinders. *J. Fluid Mech.* **251**, 687–708.
- MANIAR, H. & NEWMAN, J. N. 1997 Wave diffraction by long arrays of cylinders. *J. Fluid Mech.* **339**, 309–330.
- MCCALL, S. L., PLATZMANN, P. M., DALICHAOUCH, R., SMITH, D. & SCHULTZ, S. 1991 Microwave propagation in two-dimensional dielectric lattices. *Phys. Rev. Lett.* **67**, 2017–2020.
- MCIVER, P., LINTON, C. M. & MCIVER, M. 1998 Construction of trapped modes for wave guides and diffraction gratings. *Proc. R. Soc. Lond. A* **454**, 2593–2616.
- MEI, C. C. 1983 *The Applied Dynamics of Ocean Surface Waves*. John Wiley & Sons.
- O'HARE, T. J. & DAVIES, A. G. 1993 A comparison of two models for surface-wave propagation over rapidly varying topography. *Appl. Ocean Res.* **15**, 1–11.
- PORTER, R. & EVANS, D. V. 1999 Rayleigh–Bloch surface waves along periodic gratings and their connection with trapped modes in waveguides. *J. Fluid Mech.* **386**, 233–258.
- SIGALAS, M. M. & ECONOMOU, E. N. 1992 Elastic and acoustic wave band structure. *J. Sound Vib.* **158**, 377–382.
- TWERSKY, V. 1962 On scattering of waves by the infinite grating of circular cylinders. *IRE Trans. Antennas Propagation* **10**, 737–765.